ANL-85-74
NASA CR-175057

ANL-85-74
NASA CR-175057

EFFECTS OF A HIGH MEAN STRESS ON THE HIGH-CYCLE FATIGUE LIFE OF PWA 1480 AND CORRELATION OF DATA BY LINEAR ELASTIC FRACTURE MECHANICS

by

S. Majumdar and R. Kwasny

ARGONNE NATIONAL LABORATORY, ARGONNE, ILLINOIS

Operated by THE UNIVERSITY OF CHICAGO

for the U. S. DEPARTMENT OF ENERGY

under Contract W-31-109-Eng-38

Printed in the United States of America
Available from
National Technical Information Service
U. S. Department of Commerce
5285 Port Royal Road
Springfield, VA 22161

NTIS price codes
Printed copy: A03
Microfiche copy: A01

ANL-85-74
NASA/CR-175057

ARGONNE NATIONAL LABORATORY
9700 South Cass Avenue
Argonne, Illinois 60439

EFFECTS OF A HIGH MEAN STRESS ON THE HIGH-CYCLE FATIGUE LIFE OF PWA 1480 AND CORRELATION OF DATA BY LINEAR ELASTIC FRACTURE MECHANICS

by

S. Majumdar and R. Kwasny

Materials Science and Technology Division

November 1985

Prepared for the NASA Lewis Research Center, Cleveland, Ohio
under Interagency Order C-91113-D

EFFECTS OF A HIGH MEAN STRESS ON THE HIGH-CYCLE FATIGUE LIFE OF PWA 1480 AND CORRELATION OF DATA BY LINEAR ELASTIC FRACTURE MECHANICS*

by

Saurin Majumdar and Rolf Kwasny

ABSTRACT

High-cycle fatigue tests using 5-mm-diameter smooth specimens were performed on the single crystal alloy PWA 1480 (001 axis) at 70°F (room temperature) in air and at 1000°F (538°C) in vacuum (10^{-6} torr). Tests were conducted at zero mean stress as well as at high tensile mean stress. The results indicate that, although a tensile mean stress, in general, reduces life, the reduction in fatigue strength, for a given mean stress at a life of one million cycles, is much less than what is predicted by the usual linear Goodman plot. Further, the material appears to be significantly more resistant to mean stress effects at 1000°F than at 70°F. Metallographic examinations of failed specimens indicate that failures in all cases are initiated from micropores of sizes of the order of 30-40 μm. Since the macroscopic stress-strain response in all cases was observed to be linear elastic, linear elastic fracture mechanics (LEFM) analyses were carried out to determine the crack growth curves of the material assuming that crack initiation from a micropore (a_o = 40 μm) occurs very early in life. The results indicate that the calculated crack growth rates at an R (defined as the ratio between minimum stress to maximum stress) value of zero are approximately the same at 70°F as at 1000°F. However, the calculated crack growth rates at other R ratios, both positive and negative, tend to be higher at 70°F than at 1000°F. Calculated threshold effects at large R values tend to be independent of temperature in the temperature regime studied. They are relatively constant with increasing R ratio up to a value of about 0.6, beyond which the calculated threshold stress intensity factor range decreases rapidly with increasing R ratios. Although there are uncertainties in calculating the stress intensity factors for the specimen geometry that was tested, the derived crack growth curve, when extrapolated to moderate stress intensity region, agrees very closely with the limited crack growth test data (at the test temperature of interest) available for this material at R = 0.1. The comparison, if justified, also tends to show that the threshold stress intensity factor range may be smaller for specimens with short cracks than for those with long cracks.

INTRODUCTION

PWA 1480 is a potential candidate alloy for use in the high-pressure fuel turbine blade of the NASA space shuttle main engine. As a high-pressure turbine material, it will be subjected to vibratory high-cycle fatigue loading superimposed on a high mean stress due to centrifugal loading. The present testing program at Argonne National Laboratory was initiated by NASA Lewis Research Center to study the effects of a high mean stress on the high-cycle fatigue behavior of single-crystal PWA 1480. Since the high mean stress in an actual turbine blade of the space shuttle main engine occurs

near the root region (where temperatures are relatively low), the temperatures for testing were restricted to 70°F (room temperature) and 1000°F (538°C). To minimize the effects of oxidation, tests at 1000°F were conducted in a vacuum. Also, since the principal loading direction of interest is in the [001] direction, only specimens with their axis oriented in the [001] direction were tested.

It is known that microporosities are present in PWA 1480 and that they are often the sites of fatigue crack initiation [1]. The present study was no exception. Although there was a distribution in size, in most cases a fatigue crack was initiated from the largest (or close to the largest) microporosity present in the gauge section of the specimen. Sometimes these porosities were quite elongated and resulted in large elastic stress concentration factors. It is likely that cracks initiated from these porosities very early in life. A purpose of the present study was to investigate whether the generated data could be rationalized on the basis of a fatigue crack growth analysis. Fatigue crack growth data on single-crystal PWA 1480 are not easily available. Some data were reported in Ref. 1 for tests carried out generally at much higher temperatures than those used in the present study. In the absence of a large data base, LEFM analyses were used to estimate the fatigue crack growth rate properties necessary to obtain a good correlation between observed and calculated lives, ignoring crack initiation lives. Although there are uncertainties in the calculations because of uncertainties in the initial crack size (due to a variability in the size of the microporosity responsible for crack initiation and in the computations of stress intensity factors), the derived crack growth rates, when extrapolated to larger stress intensity factors, compare very well with the very limited experimental data available for this material.

OBJECTIVES

The primary objective of the test program was to conduct high mean stress high-cycle fatigue tests on single-crystal PWA 1480 in order to establish the effects of a high mean stress on the high-cycle fatigue life. Because of the limited scope of the program, the target life was set nominally at one million cycles. A second objective was to carry out metallographic examination of a sufficient number of failed specimens in order to establish the effects of microstructure on damage. A final objective was to establish a procedure for correlating the generated data on the basis of LEFM analyses.

MATERIAL

Straight gauge specimens [5 mm (0.2 in.) in diameter and 15 cm (6 in.) long], with the specimen axes oriented in the [001] direction, were supplied by NASA Lewis Research Center. NASA specifications called for the following heat treatment before machining:

2345°F in vacuum or protective atmosphere, 4 h, rapid air cooled +
1975°F in protective atmosphere, 4 h, air cooled

Additional aging heat treatment of 1600°F for 32 h in air followed by air cooling was given after machining of specimens. The measured elastic modulus, proportional stress limit, 0.2% offset yield stress, and ultimate tensile strength at 70°F and 1000°F are given in Table 1. Note that, in contrast to 70°F, significant strain hardening is present at 1000°F. Thus, although the proportional limit is reduced with increasing temperature, the 0.2% offset yield stress remains nearly constant.

Table 1. Mechanical Properties of As-Received PWA 1480 (001)*

Temp, °F	Elastic Modulus, x 10^{-6} psi	Proportional Limit, ksi	0.2% Offset Stress, ksi	Ultimate Tensile Strength, ksi
70	18.4	146	146	154
1000	16.6	125	144	-

*1 ksi = 6.895 MPa.

Prior to testing, each specimen was polished with 1-μm diamond paste. However, the surfaces of each specimen contained many pores, some of which were as large as 40 μm (Fig. 1).

TEST PROCEDURE

In the initial tests, specimens were subjected to axial strain controlled cycles. However, very little cyclic plasticity was observed. For example, Fig. 2 shows the hysteresis loop at the tenth cycle of a 0 to 0.8% strain cycling test at 70°F. The hysteresis loop has almost zero width and very little cyclic mean stress relaxation occurred during the test. Similar behavior was also observed at 1000°F. Since almost all the tests were conducted at much lower strain ranges, where the hysteresis loops have no measurable widths, it was decided to proceed with the testing under load-control at a frequency of 20 Hz. Because of the reduction of the proportional stress limit at 1000°F, plastic yielding occurred at the tensile end of the first cycle of the high mean stress high-cycle fatigue tests. However, the magnitude of the plastic strain is estimated to be only 0.05%, and there was no evidence of ratchetting with cycles, shakedown being reached after the first cycle.

The tests at 70°F were conducted in a laboratory air environment. In order to minimize oxidation effects, the tests at 1000°F were conducted in vacuum (8 x 10^{-7} torr). The specimens were heated by a Lepel induction heater operating at a frequency of 455 kHz.

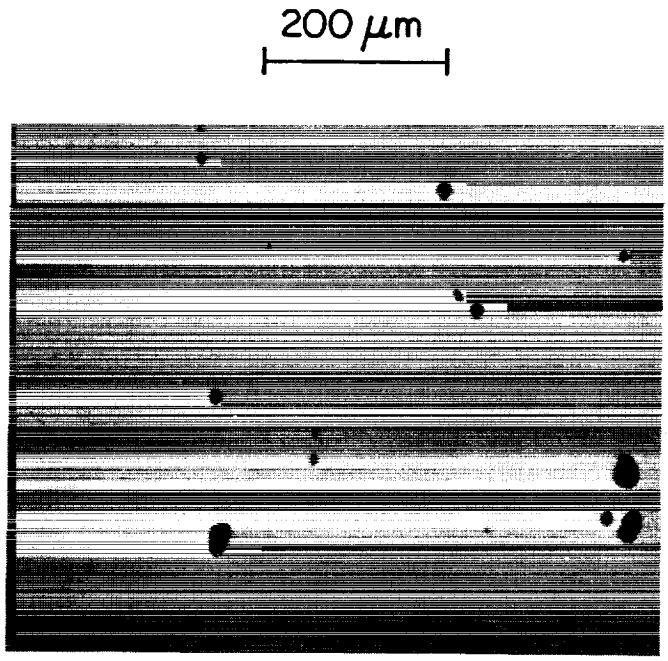

Fig. 1

Optical Micrograph Illustrates Typical Micropore Density in Unetched Specimen.

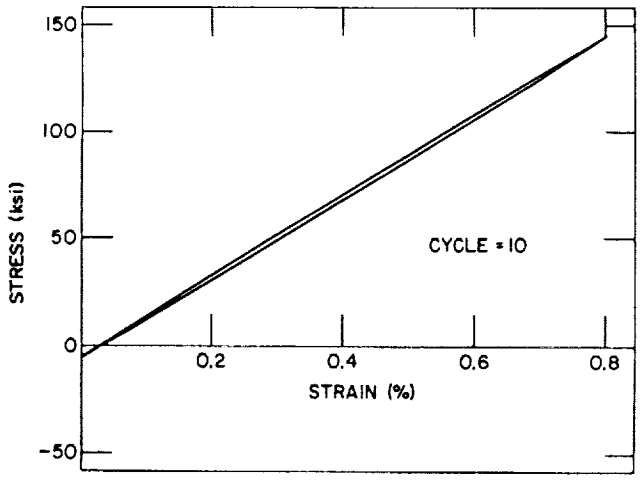

Fig. 2

Hysteresis Loop at 10th Cycle for PWA 1480 (001) Specimen Subjected to Cycling between 0 and 0.8% Strain Range at 20°C (70°F). 1 ksi = 6.895 MPa.

Since the stress ranges corresponding to the target life of a million cycles were not known a priori, testing at each mean stress was initiated by cycling for about a million cycles at an estimated stress range. Thereafter, the stress range was increased successively by about 2 ksi (15 MPa) after approximately each million cycles until the specimen failed. Barring a few exceptions, failure of the specimens always occurred at or near the center of the specimen gauge section. The fracture surfaces of a number of specimens were examined in an optical or a scanning electron microscope.

TEST RESULTS

A summary of all the tests conducted are presented in Tables 2 and 3 and in Figs. 3 and 4 for test temperatures of 70°F and 1000°F, respectively. Note that the material displays a threshold-type behavior at each temperature where the scatter in life is quite large. However, at higher stress ranges (shorter lives) the tests are quite reproducible. The Goodman diagram corresponding to a life of a million cycles estimated from these tests is shown in Fig. 5. Note that in contrast to the usual linear drop-off in stress amplitude with increasing mean stress, PWA 1480 tends to be quite resistant to mean stress effects at 70°F and somewhat less so at 1000°F. This behavior is, of course, not unique to single-crystal PWA 1480 because it has also been observed in another polycrystalline superalloy [2]. Interestingly, the fatigue strength at a given mean stress is larger at 1000°F than at 70°F, particularly at low mean stresses. The increase in strength with temperature may be a result of thermal aging.

METALLOGRAPHIC OBSERVATIONS

Several specimens were examined by optical and scanning electron microscopes after fracture. Each specimen contained a large number of micropores (Fig. 1) ranging in size from a few micrometers to as large as 40 μm and occasionally formed clusters. Crack initiation always occurred from one of these micropores, usually one of the larger ones. An example is shown in Fig. 6 for the specimen from test 1324 which was cycled at 70°F at a stress range of 60 ksi (414 MPa) with zero mean stress. A similar mode of crack initiation was also observed (Fig. 7) in the specimen from test 1336 which was cycled at 70°F at a stress range of 38 ksi (262 MPa) and a mean stress of 120 ksi (827 MPa). The pore initiating the crack is about 40-μm long and has an aspect ratio of about 3. Note that the crack is very tight and macroscopically appears to grow along crystallographic planes, possibly {111}-type planes. In both specimens, the crack that led to failure was initiated by a crack on a different slip plane (Figs. 6 and 8). Crack growth also appeared to preferentially follow microporosities (Fig. 9). (The distinct slip band marks along {111}-type of planes in the figure are for a test with a rather large (0.8%) strain range. Such slip bands were not observed in the low strain range, high-cycle fatigue test specimens.) Crack initiation in specimens tested at 1000°F also occurred at micropores. An example (test no. 1347) is shown in Fig. 10, where the crack initiated at a cluster of microporosities with a major axis of at least 150 μm. The crack propagated radially on what appeared to be a {111} plane.

Table 2. Summary of Tests on PWA 1480 at 20°C (70°F) in Air (1 ksi = 6.895 MPa)

Test No.	Stress, ksi		R	Frequency, Hz	Cycles to Failure	Remarks
	Range	Mean				
1317	160	+71	0	1	5,900	Strain controlled 0↔0.8%
1318	151	-7	-1.2	1	21,800	Strain controlled ±0.4%
1319	96	+3	-0.88	1	138,500	Strain controlled ±0.25%
1320	56	0	-1	1[a]	2.73×10^6	Failed at bottom gauge mark
1324	60	0	-1	20	2.33×10^6	Failed
1321	20	+120	0.85	20	6.75×10^6	Increase stress range
	30	+120	0.78	20	7.95×10^6	Failed
1322	30	+120	0.78	20	12.29×10^6	Increase stress range
	40	+120	0.71	20	12.59×10^6	Failed
1325	40	+120	0.71	20	369,700	Failed 1/8" above top gauge mark
1336	38	+120	0.73	20	768,400	Failed
1326	60	60	0.33	20	159,400	Failed just above top gauge mark
1328	60	60	0.33	20	141,700	Failed
1329	44	60	0.46	20	25.45×10^6	Decrease stress range
	40	60	0.50	20	27.18×10^6	Increase stress range
	44	60	0.46	20	32.60×10^6	Increase stress range
	45	60	0.45	20	41.25×10^6	Increase stress range
	46	60	0.45	20	44.83×10^6	Increase stress range
	47	60	0.44	20	48.13×10^6	Increase stress range
	48	60	0.43	20	48.87×10^6	Failed

[a]Switched to 20 Hz after 1.2×10^6 cycles.

Several slight differences were observed between specimens with zero and high mean stress. The specimen with high mean stress (test no. 1336) appeared to have cracks initiated at several sites, whereas the zero mean stress test (test no. 1324) had a single crack origin. The high mean stress specimen also had a rougher, more-textured fracture surface, which may be indicative of a higher crack propagation rate. It also contained several "steps" on the fracture surface (Fig. 8). These steps were probably caused either by the linking of two parallel cracks on the same type of octahedral plane or by the intersection of cracks on nonparallel octahedral planes.

LEFM ANALYSIS

Since fracture in all cases initiated from one of the micropores which often were elongated, and since the macroscopic stress strain response for all the tests was essentially linear, LEFM analyses seemed appropriate. However, one complicating factor was that PWA 1480 single crystals are anisotropic and consequently the crack did not grow in a pure mode I fashion because crack growth was often crystallographic along {111}-type planes (Fig. 11). This is in contrast to the usual experience [3] in testing isotropic polycrystalline materials in mixed-mode fatigue, where the crack

Table 3. Summary of Tests on PWA 1480 at 538°C (1000°F) in Vacuum (1 ksi = 6.895 MPa)

Test No.	Stress, ksi		R	Freq., Hz	Cycles	Remarks
	Range	Mean				
1346[a]	30	105	0.75	1	7×10^4	Increase frequency
	30		0.75	10	2.63×10^6	Increase stress range
	32		0.74	12	3.68×10^6	Increase stress range
	34		0.72		4.70×10^6	Increase stress range
	36		0.71		5.75×10^6	Increase stress range
	38		0.69		6.79×10^6	Increase stress range
	40		0.68		7.21×10^6	Failed[b]
1347	40	105	0.68	6	2.52×10^6	Increase frequency
	40		0.68	20	9.93×10^6	Increase stress range
	42		0.67		14.64×10^6	Increase stress range
	44		0.65		16.34×10^6	Increase stress range
	46		0.64		18.03×10^6	Increase stress range
	48		0.63		19.11×10^6	Failed
1350	50	105	0.62	20	0.65×10^6	Failed
1351	50	105	0.62	20	1.11×10^6	Failed
1353	90	60	0.14	20	8.06×10^4	Failed
1354	58	60	0.35	20	6.04×10^5	Failed
1364	65	0	-1	20	9.36×10^5	Failed[b]
1383	66	0	-1	20	6.79×10^6	Increase stress range
	68	0	-1	20	8.61×10^6	Increase stress range
	70	0	-1	20	10.17×10^6	Increase stress range
	72	0	-1	20	10.57×10^6	Failed[b]
1384	90	0	-1	10	6.10×10^5	Failed

[a]This specimen had a 0.004-in. taper. All other specimens had a 0.010-in. taper.

[b]The specimen failed in the thermocouple region.

eventually turns and propagates in a pure mode I fashion. Assuming a 2-dimensional edge crack of length a in a {111}-type plane subjected to a uniaxial stress σ in the [001] direction, it is easy to show that the modes I and II stress intensity factors in an isotropic material are given by

$$K_I = 1.12 \times 2/3\ \sigma \times [\pi a]^{\frac{1}{2}} \tag{1}$$

and

$$K_{II} = 1.12 \times 1/3\ \sigma \times [\pi a]^{\frac{1}{2}} \tag{2}$$

The effective stress intensity factor for such a configuration is some function of K_I and K_{II} which is not known for this single-crystal material. For example, if the effective K is taken as

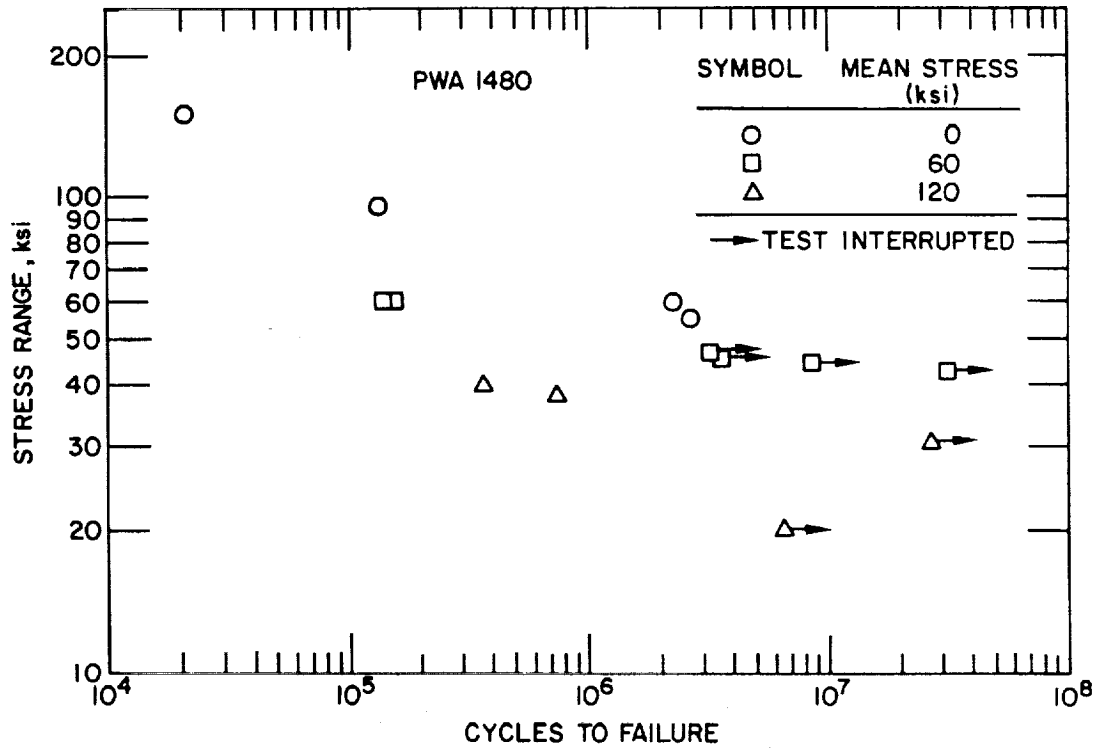

Fig. 3. Summary of High-cycle Fatigue Tests of PWA 1480 (001) at 20°C (70°F) at Various Mean Stresses. 1 ksi = 6.895 MPa.

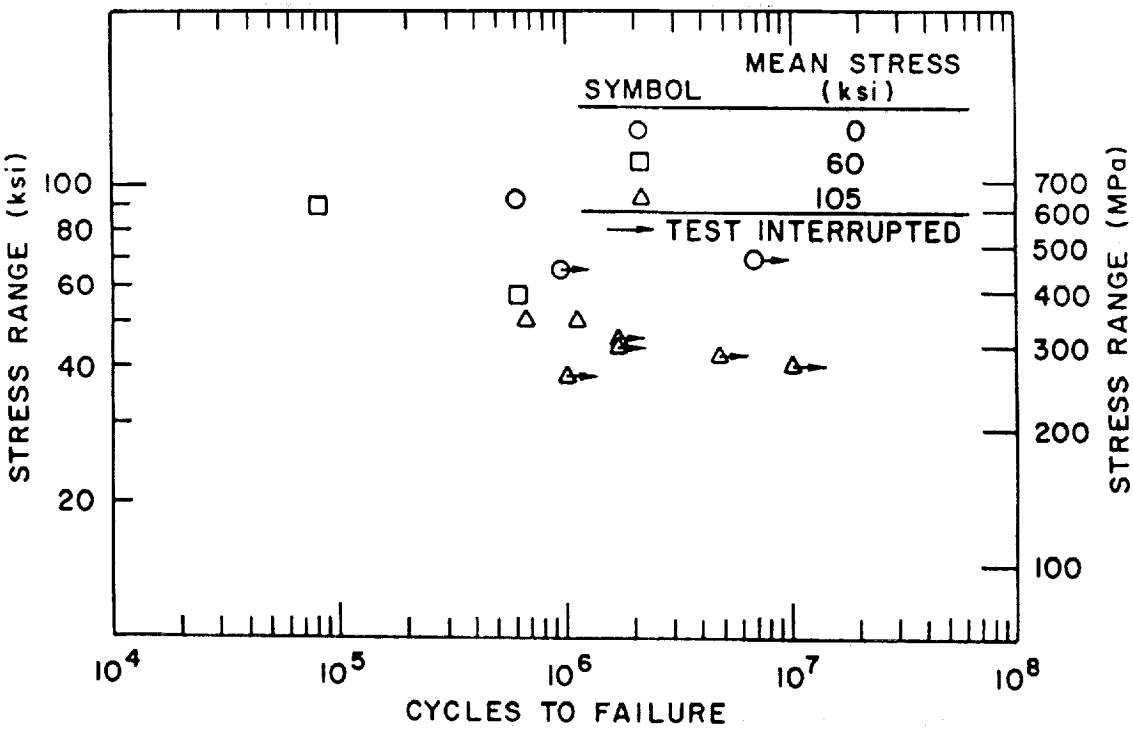

Fig. 4. Summary of High-Cycle Fatigue Tests on PWA 1480 (001) at 538°C (1000°F) at Various Mean Stresses.

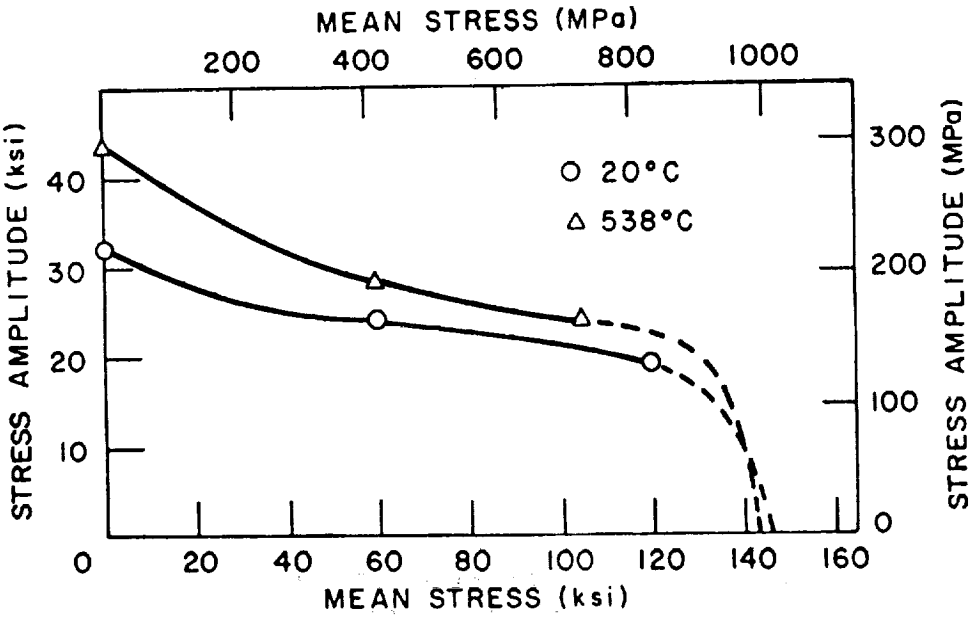

Fig. 5

Goodman Diagram for PWA 1480 (001) at 20°C (70°F) and at 538°C (1000°F).

$$K_{EFF} = \left(K_I^2 + K_{II}^2\right)^{\frac{1}{2}} , \tag{3}$$

then the crack driving force for the case in hand is

$$K_{EFF} = 1.12\left(\frac{\sqrt{5}}{3}\,\sigma\right)[\pi a]^{\frac{1}{2}} , \tag{4}$$

which, considering that the crack is not really 2-dimensional but is of a thumbnail type (modes I, II, and III), is sufficiently close to the expression for a pure mode I crack under a stress σ,

$$K_I = 1.12\sigma\,[\pi a]^{\frac{1}{2}} . \tag{5}$$

Because of simplicity and considering all the uncertainties involved, Eq. (5) is used as the expression for K in the following analyses, bearing in mind that the calculated stress intensity factors may be consistently off by some unknown (possibly close to 1) constant factor. The uncertainty in using Eq. (5) caused by the anisotropy of the material needs to be resolved in the future.

The fatigue crack growth rate, da/dN, is then assumed to follow a power law equation,

$$\frac{da}{dN} = \begin{cases} C[u(R)\Delta K]^n & \text{for} \quad \Delta K > \Delta K_{th} \\ 0 & \text{for} \quad \Delta K < \Delta K_{th} \end{cases} , \tag{6}$$

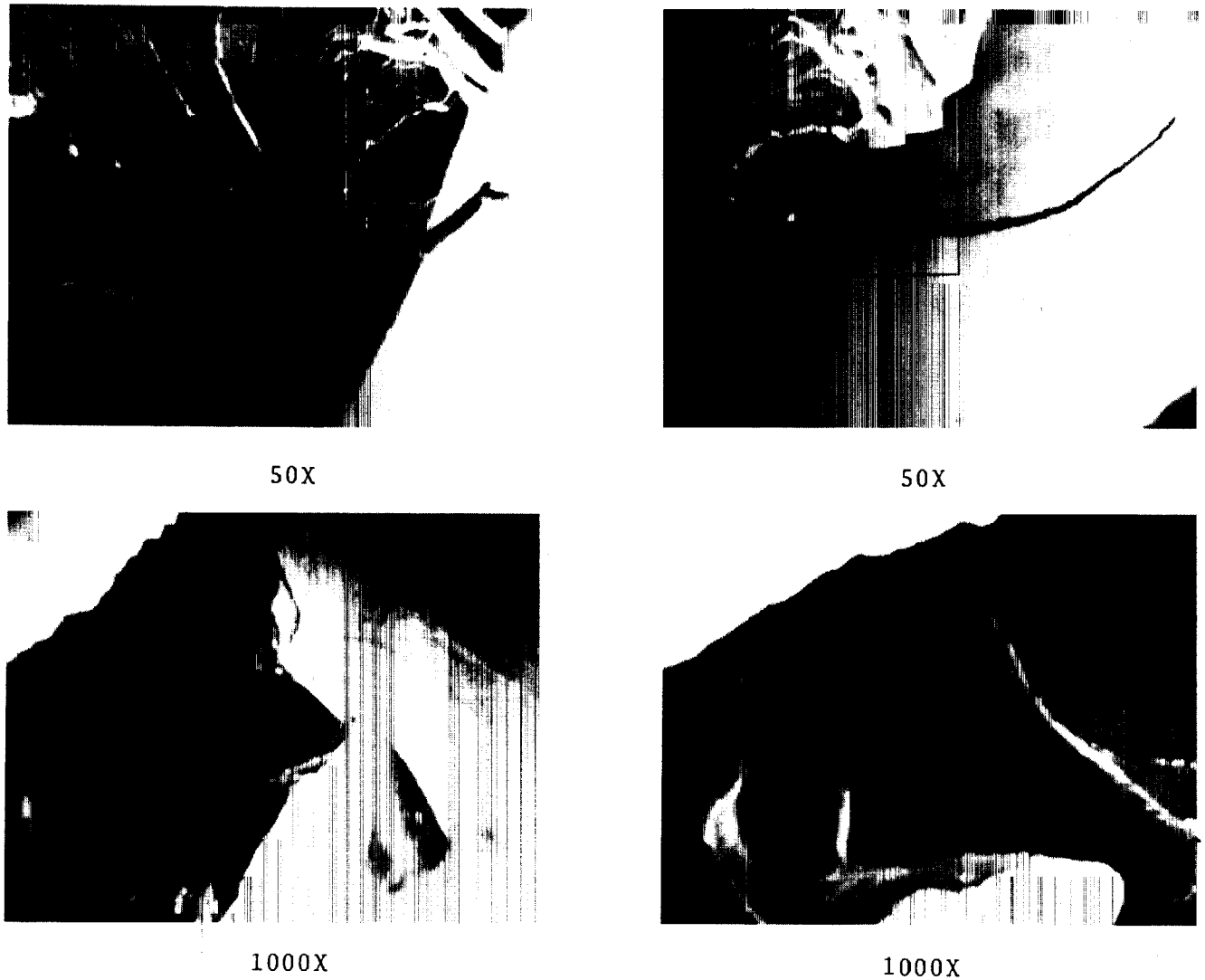

Fig. 6. Fracture Morphology in Specimen That was Cycled at a Stress Range of 60 ksi (414 MPa) with Zero Mean Stress at 20°C. The micropore initiated two cracks on different planes; one of these cracks led to failure of the specimen.

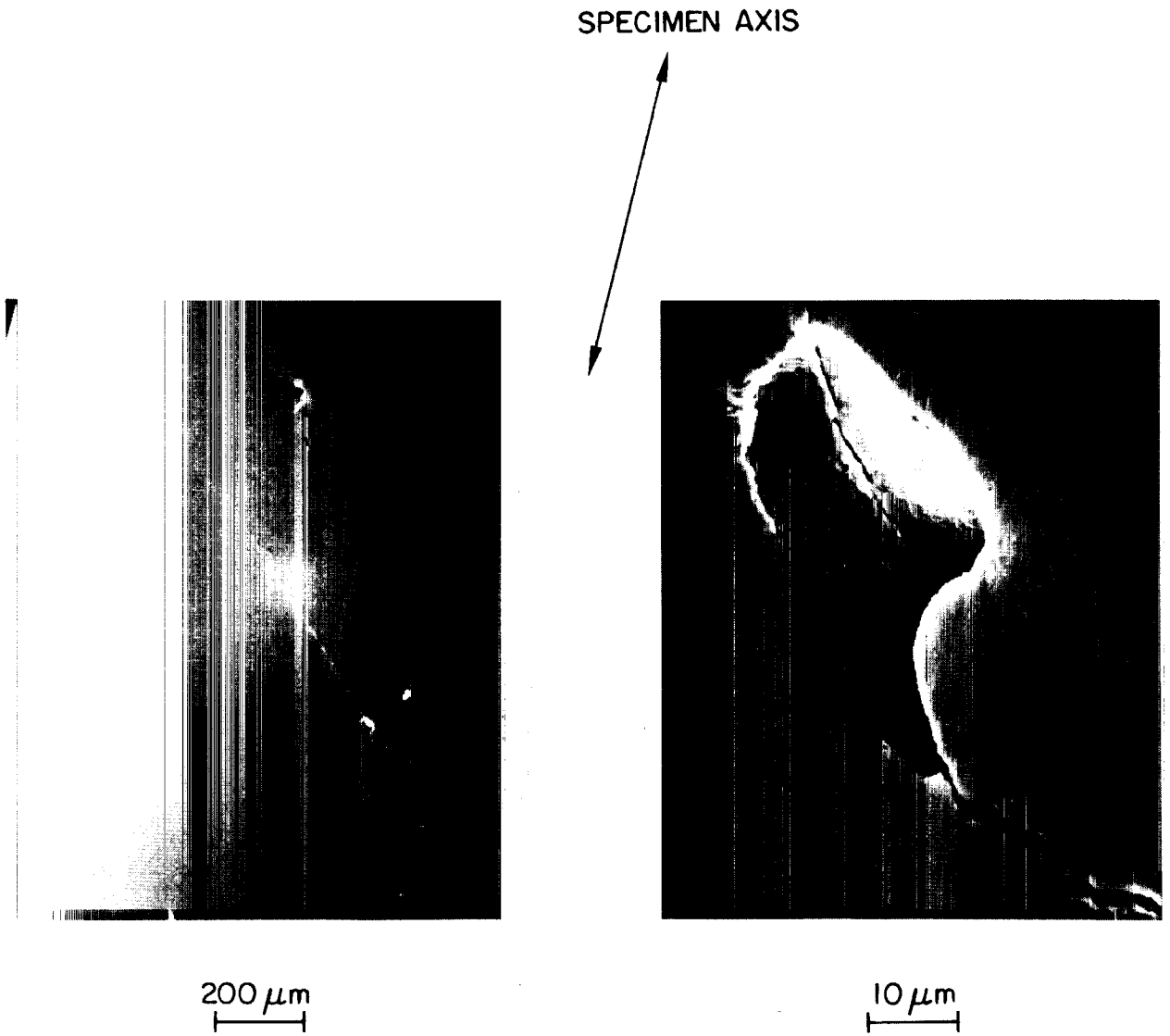

Fig. 7. Scanning Electron Micrographs Showing Surface Pore from Which Crack Was Initiated under High-cycle Fatigue Loading with Stress Range of 38 ksi (262 MPa) and Mean Stress of 120 ksi (827 MPa) at 20°C (70°F).

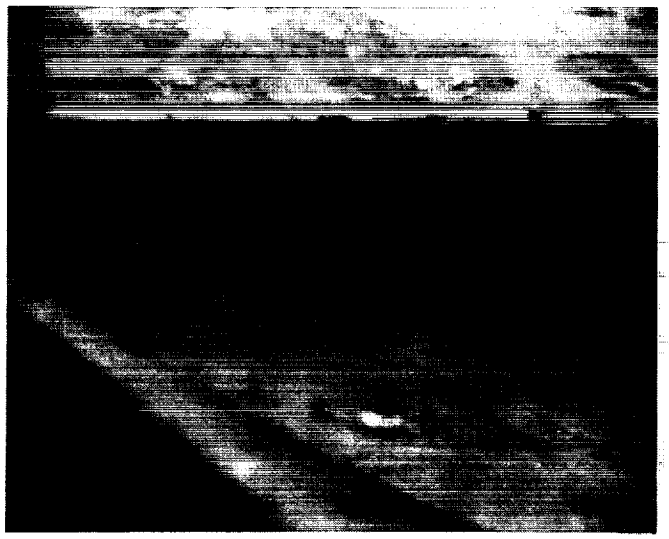

Fig. 8

Scanning Electron Micrograph Shows a "Stepped" Fracture Surface in a Specimen That Was Cycled at a Stress Range of 38 ksi (262 MPa) with Mean Stress of 120 ksi (827 MPa) at 20°C (70°F).

ΔK = stress intensity factor range,

ΔK_{TH} = threshold stress intensity factor range,

R = ratio of minimum to maximum stress in the cycle,

$u(R)$ = a factor to account for mean stress effects.

The cycles to failure for a loading above the threshold regime can then be simply obtained by integration,

$$N_f = \int_{a_o}^{a_f} \frac{da}{C[u(R)\Delta K]^n} , \qquad (7)$$

where a_o is the initial crack size (∿40 μm) and a_f is the final crack size (∿2-3 mm). Unfortunately, the material constants for this material at the temperatures of interest (70 and 1000°F) are not available. Limited crack growth data at 800°F are reported in Ref. 1. However, these data were generated at much larger stress intensity values than are required for the present analyses.

Therefore, instead of calculating life directly from Eq. (7), it was decided to compute the necessary crack growth rate properties from the limited smooth specimen data generated in this program using the following assumptions:

1. Ignore crack initiation life.

2. Compute the coefficient C and exponent n in Eq. (6) from fully reversed tests at 70°F.

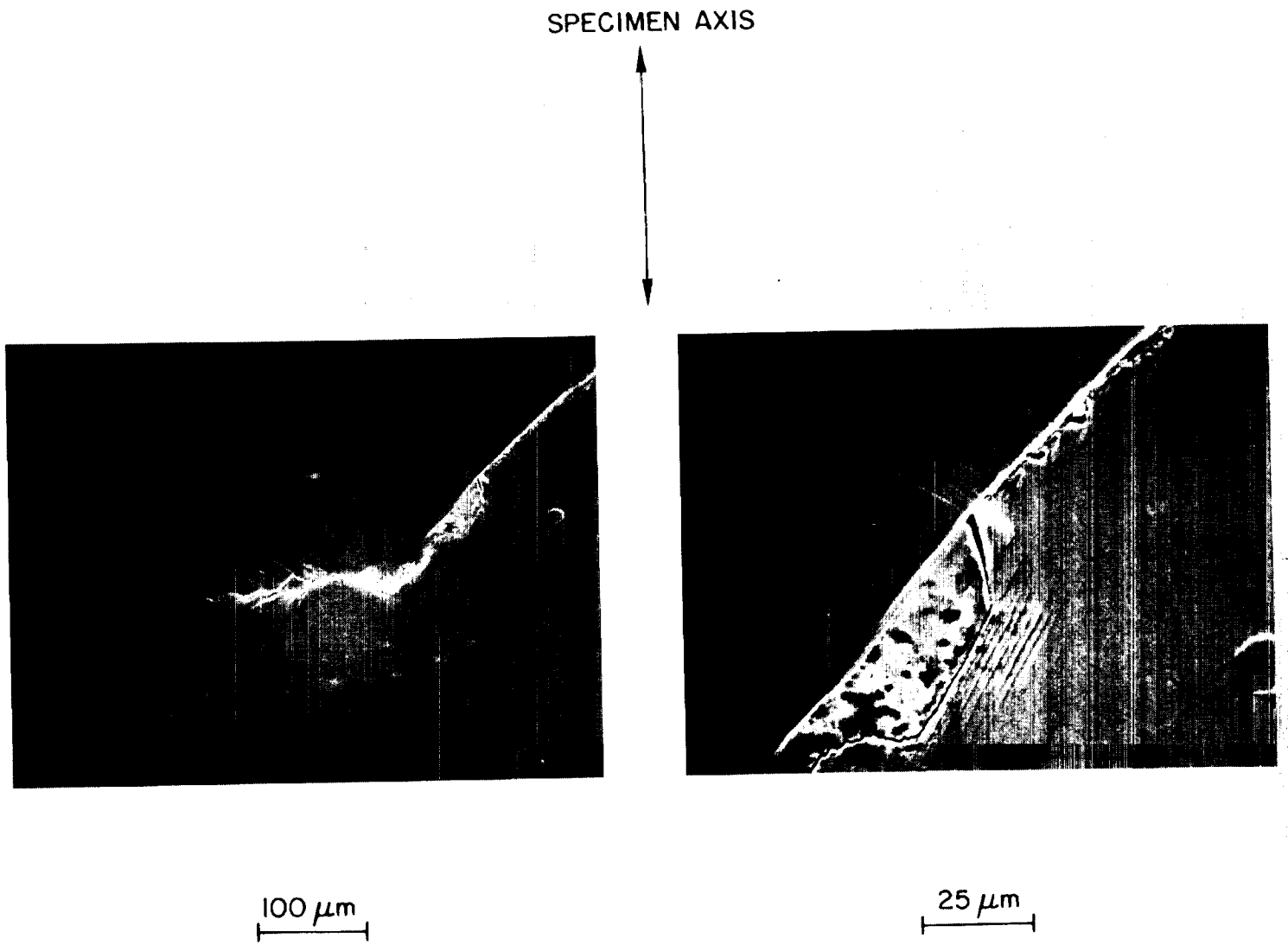

Fig. 9. Scanning Electron Micrographs Showing Crack Propagation in PWA 1480 under 0 to 0.8% Strain Range Testing at 20°C (70°F).

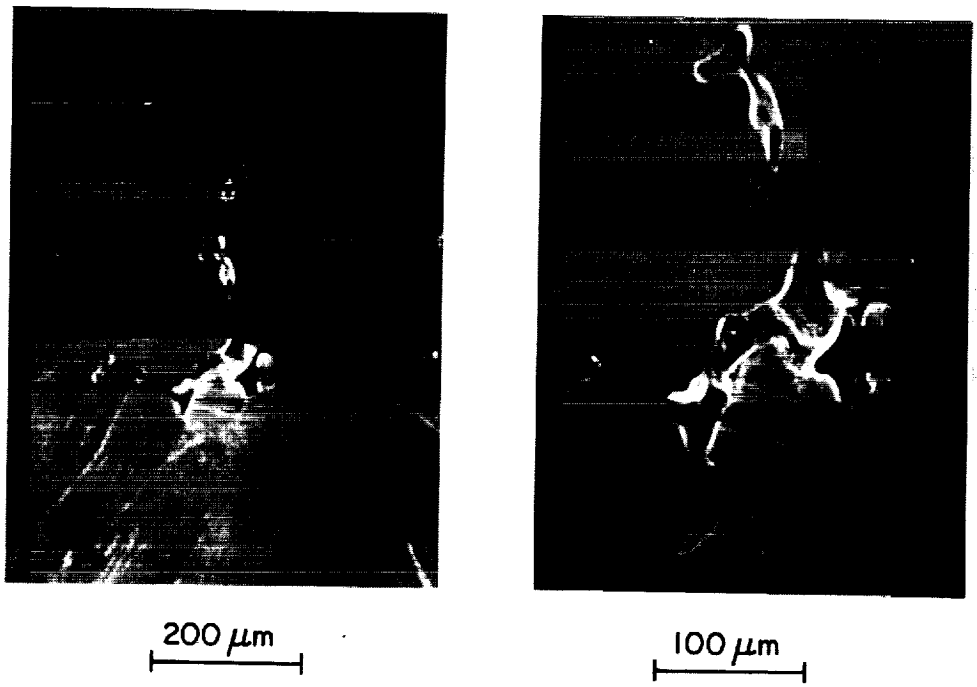

Fig. 10. Micrograph of a PWA 1480 Specimen Tested at 538°C (1000°F), Showing Crack Initiation from a Cluster of MIcropores.

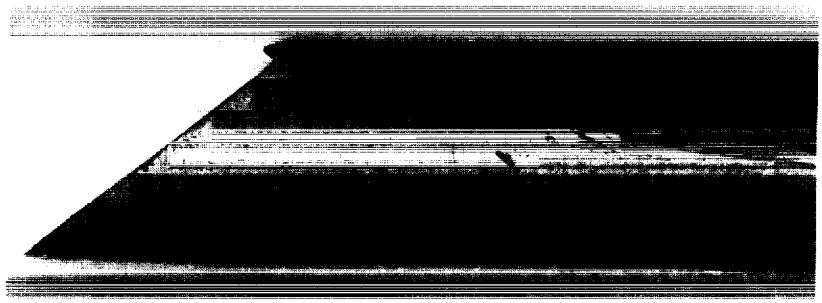

Fig. 11. Typical Crystallographic Fracture of PWA 1480 (001) Due to High-Cycle Fatigue.

3. Assume the exponent n to be independent of temperature and R ratio.

4. Determine u(R) and $\Delta K_{TH}(R)$ from correlation with the lives at high mean stress tests.

5. Assume initial and final crack sizes to be 40 μm and 2 mm, respectively. The results are insensitive to the actual value of the final crack size.

A simple integration of Eq. (7) for cycling at a constant stress range and R value gives ($n \neq 2$)

$$N_f = \frac{a_o^{1-n/2} - a_f^{1-n/2}}{(n/2 - 1)\, C[1.12\sqrt{\pi}\, \Delta\sigma u(R)]^n} . \tag{8}$$

A least-squares fit to the life data at R = -1 (fully reversed cycles) gives (Fig. 12)

$$N_f = 3.03 \times 10^{19}\, \Delta\sigma^{-5.04} \quad (\Delta\sigma \text{ in MPa}) . \tag{9}$$

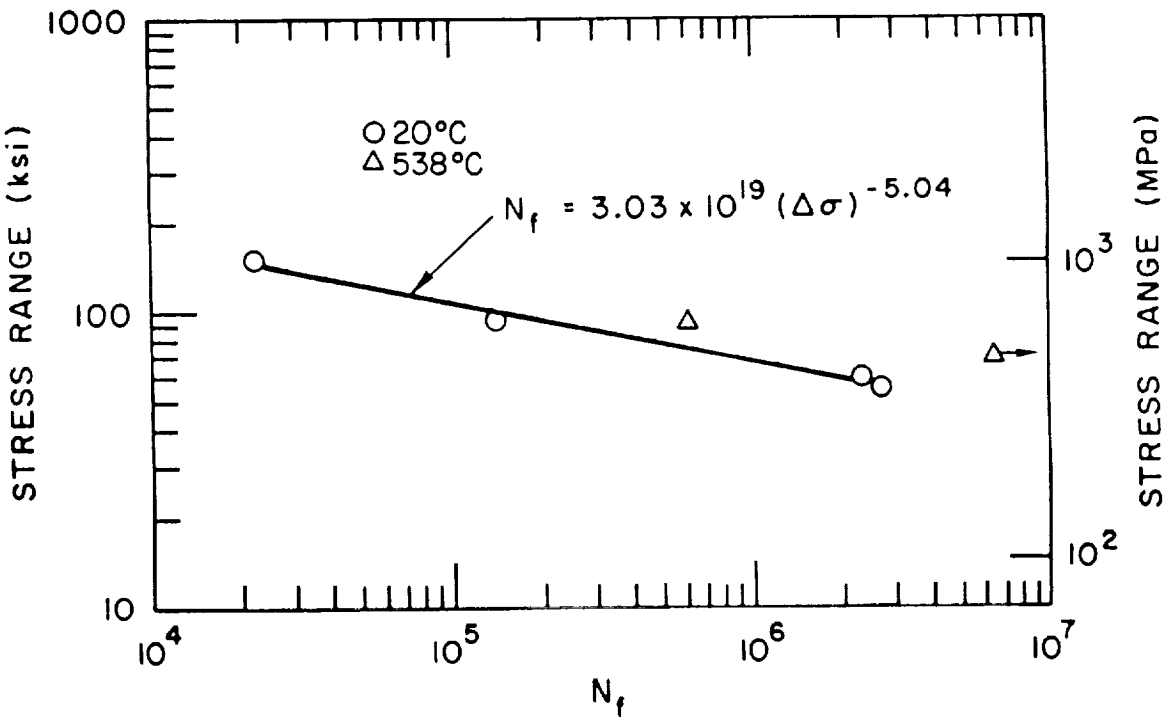

Fig. 12. Zero Mean Stress High-Cycle Fatigue Test Data on PWA 1480.

A comparison of Eqs. (8) and (9) gives n = 5.04. Normalizing u(R) such that u(0) = 1, and comparing Eqs. (9) and (10),

$$N_f = 1.258 \times 10^{19} \left(\frac{40 \times 10^{-6}}{a_o} \right)^{1.52} [\Delta\sigma\, u(R)]^{-5.04} \qquad (10)$$

where a_o is the initial crack size in meters. A quick calculation shows that Eq. (10) is approximately valid at 1000°F for R = 0 [u(0) = 1]. Equation (10) can then be used to compute the values of u(R) as a function of R from all the high-cycle fatigue tests run, and the results are shown in Fig. 13. Note that although the function u(R) increases linearly with R value at 1000°F, at 70°F it increases much more rapidly at positive R values.

Assuming that $a_o = 40 \times 10^{-6}$ m, and noting Eqs. (8), and (10), Eq. (6) can be written as

$$\frac{da}{dN} = 7.94 \times 10^{-15} [\Delta K\, u(R)]^{5.04} \text{ for } \Delta K > \Delta K_{th} . \qquad (11)$$

where ΔK_{th} is as yet to be determined.

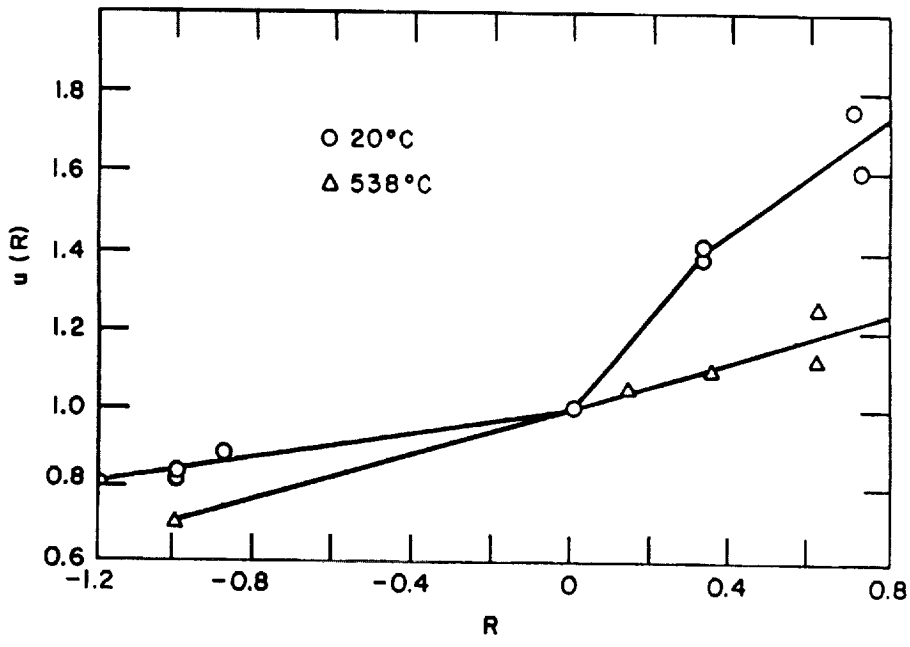

Fig. 13

Variation of the Mean Stress Correction Factor u(R) as a Function of R Ratio at 20°C (70°F) and at 538°C (1000°F).

Block Loading:

Consider the case where the material is subjected to block loading, i.e.,

$$\Delta\sigma = \Delta\sigma_i \text{ for } N_i \text{ cycles}, \quad i = 1,2, \ldots N \tag{12}$$

where the cycles N_1, N_2, ... N_N are applied sequentially. Assuming that Eq. (6) is valid for each block loading so that for the ith block, (assuming $\Delta K_i > \Delta K_{th}$)

$$a_{i-1}^{1-n/2} - a_i^{1-n/2} = C(n/2 - 1)[1.12\sqrt{\pi}\ \Delta\sigma\ u(R_i)]^n\ N_i \tag{13}$$

Summing Eq. (13) for i = 1,2, ... N, it is easy to show that failure occurs when the following linear damage rule is satisfied:

$$\sum_{i=1}^{N} \frac{N_i}{N_{f_i}} = 1 \tag{14}$$

where N_{f_i} = the cycles to failure under constant loading corresponding to the ith block. Of course, Eq. (14) is not applicable, in general, because of threshold and crack growth retardation effects. However, in all applications where the loading is never reduced from one block to the next and where transient effects can be neglected, Eq. (14) will still be applicable provided the value of N_{f_i} is set equal to infinity for blocks whose loadings correspond to ranges of stress intensity factor below the threshold value.

Threshold Stress Intensity Factor Range:

Since all the tests were conducted on nominally smooth specimens without any macroscopic starter cracks, it was impossible to distinguish between an endurance limit for crack initiation from a true threshold effect for crack propagation. Such a distinction can only be made by conducting interrupted tests and examining the specimens for cracks. In the absence of such detailed information, it is assumed that crack initiation at the tip of the largest porosity is always possible and that the tests involving runouts were truly indicative of threshold effects. A determination of the threshold stress intensity factor range can be attempted from an analysis of the block load tests tabulated in Tables 2 and 3. Threshold stress intensity factor of PWA 1480 for the present purposes will be defined as the stress intensity factor range below which the exponent in Eq. (11) is significantly above 5.04 so that a straightforward application of Eq. (14) grossly underestimates the lives. Of course, the calculated threshold stress intensity factor range will depend on the size of the initiating micropore. However, since cracks initiated from micropores in size of the order of 40 μm in most cases where the specimens were examined, it was assumed that the initiated crack size in all specimens is 40 μm. The error involved in such an assumption can be estimated from the square root dependency of the calculated threshold stress intensity factor range on the initial crack size. Figure 14 shows the estimated ranges of threshold stress intensity factor as a function of R ratio at

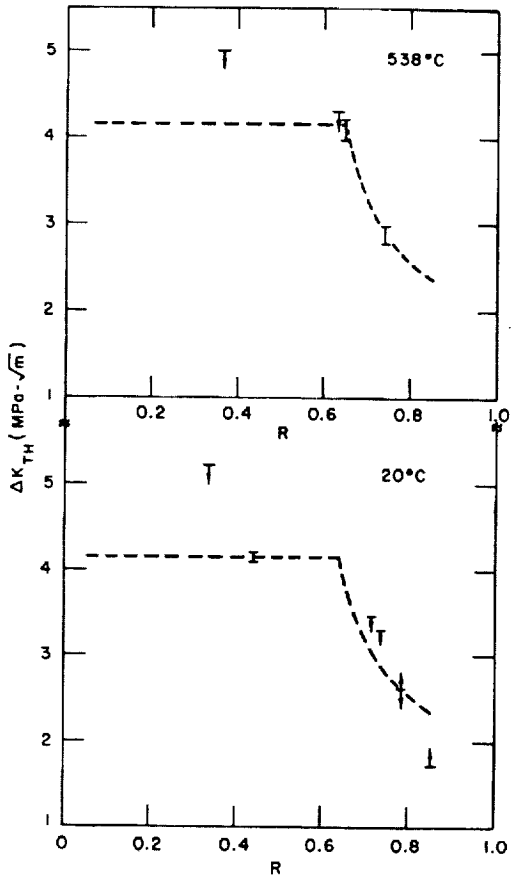

Fig. 14

Variation of the Threshold Stress Intensity Factor Range with R Ratio at 20°C (70°F) and 538°C (1000°F).

70°F and at 1000°F. Data are too scarce to unambiguously determine the variation of threshold values with R. Dashed lines (independent of temperature) are included as possible variations of threshold stress intensity factor range with R ratio that are consistent with the calculated ranges. It appears that the threshold stress intensity factor range is relatively independent of R ratio up to about 0.6, beyond which it drops off rapidly with increasing R. Also, within the accuracy of the present calculations there appears to be no significant effect of temperature on threshold at positive R values between 70 and 1000°F. However, at R = -1 the threshold stress intensity factor is greater at 1000°F than at 70°F.

DISCUSSION

The calculated cycles to failure on the basis of crack growth (ignoring crack initiation) are compared with experimentally observed cycles to failure for all the tests (including block load tests) in Fig. 15. For block load tests, observed and calculated cycles include only those blocks for which a nonzero crack growth is predicted. Otherwise the comparison would be much more favorable on a total cycles basis. Note that the correlation is equal to or better than a factor of two in most cases. This, of course, does not prove that crack initiation life is negligible in this material. To prove that will require a lot more metallographic work using interrupted tests. The purpose of this exercise is to show that a credible analysis of the data can be made using LEFM.

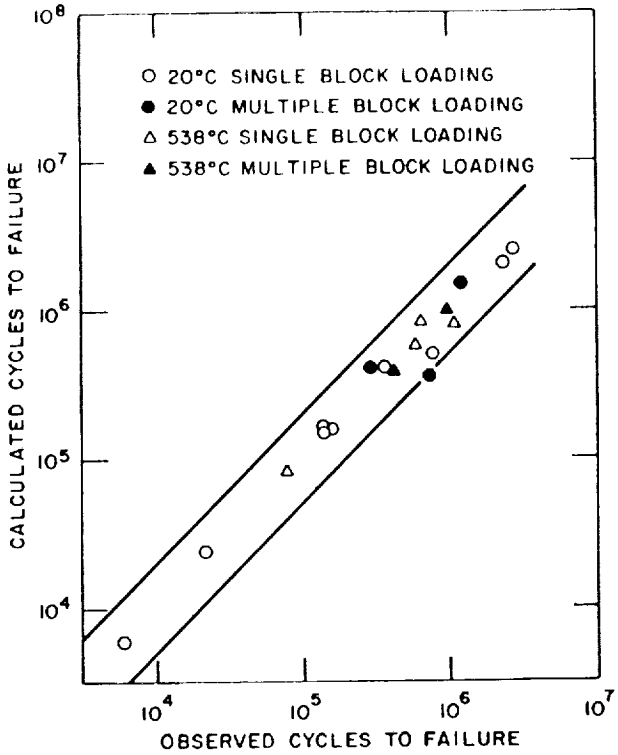

Fig. 15

Comparison of Calculated Versus Observed Cycles to Failure.

A comparison between the crack growth rates deduced from the present exercise and the limited crack growth data reported in Ref. 1 is shown in Fig. 16. The excellent agreement both in slope and magnitude may be fortuitous for two reasons. First, there is some uncertainty in the calculations of stress intensity factors in the present study as discussed earlier. Second, the crack growth data reported in Ref. 1 are for large cracks growing in the [010] direction in a pure mode I fashion, whereas the cracks in the present study are much shorter and grow principally along {111} type planes in a mixed-mode fashion. However, the limited data in Ref. 1 showed that crystallographic effects on the crack growth rates are not very large. Finally, the test data [1] shown in Fig. 16 were obtained from crack growth tests conducted in air at 800°F whereas the tests in the present studies were conducted in vacuum at 1000°F. However, the environmental effects at these temperatures are not expected to be very large. In spite of these reservations, it is evident that the limited crack growth rate data and the derived crack growth rates in the present study are quite consistent in the moderate ΔK regime, which enhances the credibility of using LEFM to correlate the present life data.

The calculated effects of R ratio on the crack growth rates at 70°F in air and at 1000°F in vacuum are shown in Figs. 17 and 18, respectively. Crack growth rate at any ΔK value increases with increasing positive R ratio, with the increase being somewhat larger at 70°F than at 1000°F. The calculated effects of temperature on the threshold stress intensity factor range at positive R values is minimal. However, the threshold stress intensity factor range decreases rapidly with increasing R ratio beyond a value of $R = 0.6$. The effects of R ratio on crack growth rates and on threshold stress intensity factor range are in agreement with similar behavior for other material [4]. Although the calculated data are broadly in agreement with the experimental data reported in Ref. 1, there are some significant

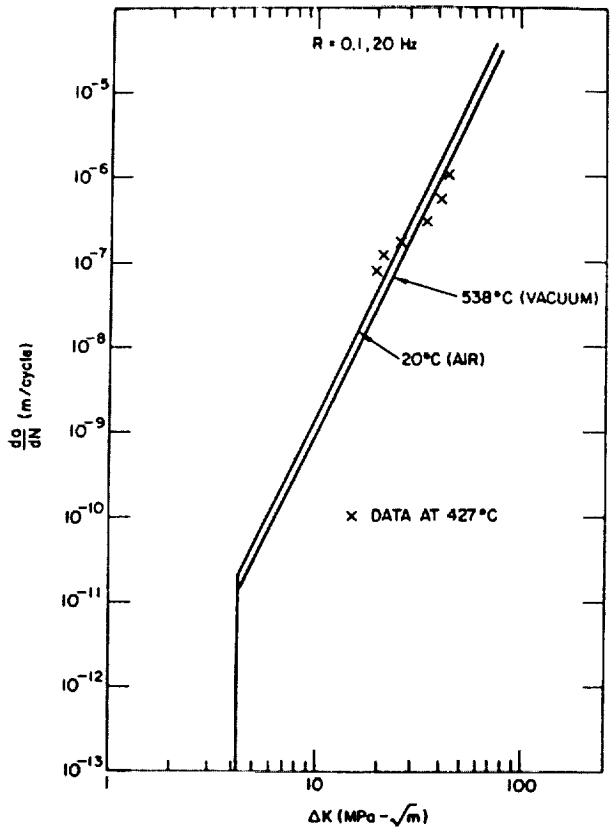

Fig. 16

Comparison of Derived Crack Growth Rates at 20°C (70°F) and at 538°C (1000°F) with Experimentally Observed Crack Growth Rate at 427°C (800°F) in PWA 1480 (001).

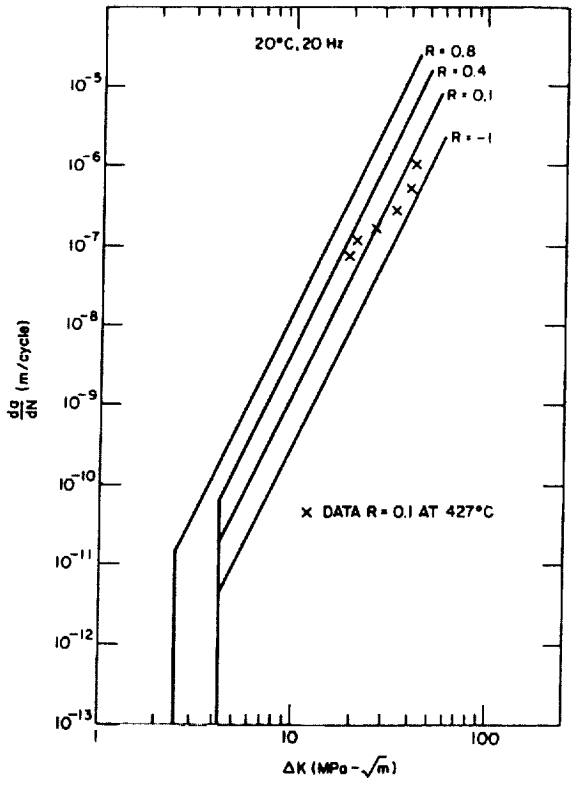

Fig. 17

Variation of the Derived Crack Growth Rate with R Ratio at 20°C (70°F).

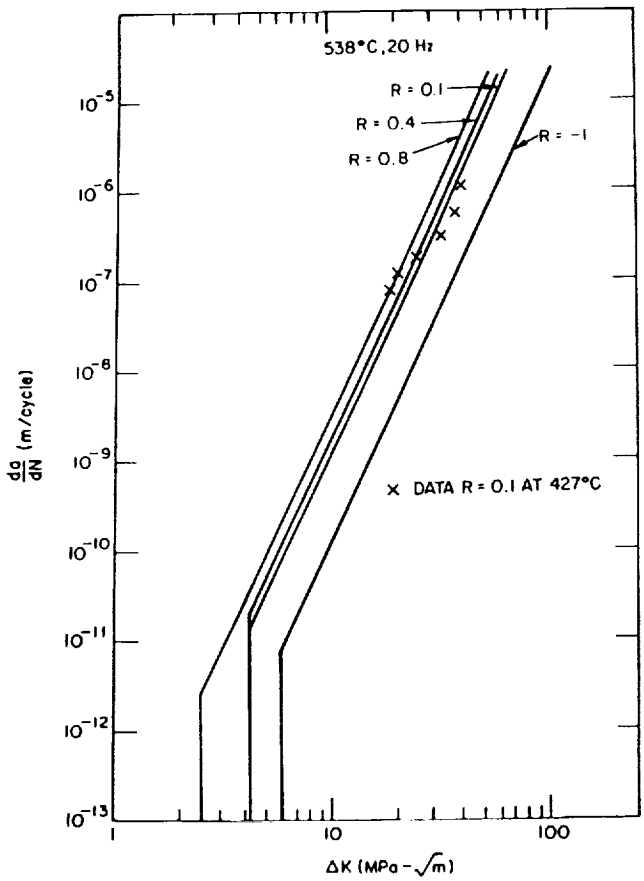

Fig. 18

Variation of the Derived Crack Growth Rate with R Ratio at 538°C (1000°F).

differences between the two. In contrast to the calculated results, the experimental data show a slight increase in crack growth rate from R = 0.1 to R = -1. However, the experiments were conducted at a higher temperature 1400°F (760°C). Also, the experimental threshold stress intensity factor at 1800°F (982°C) at R = 0.1 and at a frequency of 0.167 Hz is of the order of 10 MPa$\sqrt{m}$, which is significantly higher than the estimated value of 4 MPa$\sqrt{m}$ at 20 Hz at 1000°F in the present study. The reason for these differences was not established. It is suspected that the large difference in crack size is partially responsible.

It is interesting to speculate on the improvement of the fatigue life of PWA 1480 achieveable by controlling the size of the microporosities. First, it should be remembered that the tail end (at the large size) of the size distribution of the microporosities rather than their average size will control fatigue life. Thus, if the distribution at the tail end can be improved such that the maximum size of the porosity is reduced significantly below the existing 40 μm, significant improvement in high-cycle fatigue properties may be expected. This is shown in Fig. 19 by means of an example where the maximum size of the porosity is reduced successively from 40 to 10 μm. Note that, although life is extended even at the low-cycle end, the major benefit to be derived from reducing the maximum size of the porosity is at the high-cycle end.

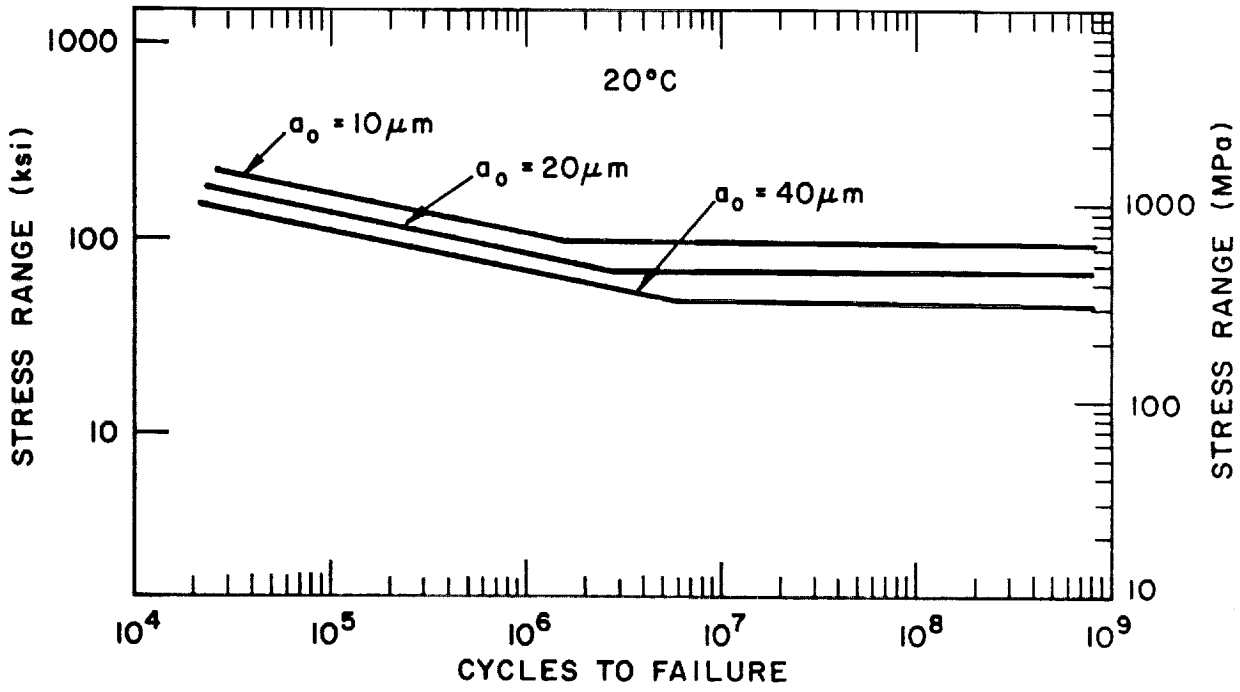

Fig. 19. Possible Improvements in the High-Cycle Fatigue Properties of PWA 1480 (001) by Controlling the Largest Size Porosity to Three Different Values.

CONCLUSIONS

1. High mean stress high-cycle fatigue tests on smooth single-crystal PWA 1480 specimens (001 axis) were carried out. The results show that the material is quite resistant to mean stress effects at 70°F (room temperature) in air and less so at 1000°F in vacuum.

2. The stress-strain response in all the tests was linear elastic, and no significant cycle-dependent creep was observed in any of the high mean stress tests. The material displayed very little strain hardening at 70°F, but significant strain hardening was evident at 1000°F.

3. Metallographic studies on failed specimens showed cracks to be nucleated from microporosities of size of the order of 40 μm.

4. Crack propagation occurs crystallographically along {111}-type planes in a combined mode I and II fashion.

5. LEFM analyses, ignoring crack initiation life, were used to derive crack growth rates for the material. When extrapolated to moderate ΔK regime, the computed crack growth rates compare quite favorably with limited data available for this material.

6. The computed crack growth rate at a given ΔK decreases as the temperature increases from 70°F to 1000°F and increases with increasing R ratio, the increase being more pronounced at 70°F than at 1000°F.

7. The computed crack growth also shows a threshold behavior which is independent of temperature between 70 and 1000°F at positive R values. The threshold stress intensity factor range (ΔK_{TH}) is relatively independent of R ratio up to a value of R = 0.6, beyond which it drops rapidly with increasing R. The computed ΔK_{TH} at R = 0.1 is significantly smaller than the experimentally observed value, which implies that ΔK_{TH} may be dependent on crack size.

8. Significant improvement in fatigue strength, particularly at the high-cycle end, is theoretically possible by controlling the maximum size of the porosities.

ACKNOWLEDGMENTS

The authors would like to thank Professor S. Antlovich and Mr. W. Mulligan of Georgia Institute of Technology for providing Figs. 1, 6, 8, and 10.

REFERENCES

1. D. P. DeLuca and B. A. Cowles, Fatigue and Fracture of Advanced Blade Materials, Final Report for Period 1, August 1982 through August 31, 1984, Materials Laboratory, Air Force Wright Aeronautical Laboratories Report ASD-86-0051 (AFSC) (February 1985).

2. D. M. Moon and G. P. Sabol, "Effect of Mean Stress on the High-cycle Fatigue Behavior of Udimet 710 at 1000°F," in Fatigue at Elevated Temperatures, ASTM STP 520, American Society for Testing and Materials, pp. 438-450 (1973).

3. R. Badaliance, "Mixed Mode Fatigue Crack Propagation," in Mixed Mode Crack Propagation, Ed. G. C. Sih and P. S. Theocaris, Sijthoff and Noordhoff, pp. 77-98 (1981).

4. C. Amzallag, P. Rabbe, C. Bathias, D. Benoit, and M. Truchon, "Influence of Various Parameters on the Determination of the Fatigue Crack Arrest Threshold," in Fatigue Crack Growth Measurement and Data Analysis, ASTM STP 738, American Society for Testing and Materials, pp. 29-44 (1981).

1. Report No.	2. Government Accession No.	3. Recipient's Catalog No.
NASA/CR-175057		

4. Title and Subtitle	5. Report Date
Effects of a High Mean Stress on the High Cycle Fatique Life of PWA 1480 and Correlation of Data by Linear Elastic Fracture Mechanics	November 1985
	6. Performing Organization Code
7. Author(s)	8. Performing Organization Report No.
S. Majumdar and R. Kwasny	ANL-85-74
	10. Work Unit No.
9. Performing Organization Name and Address	11. Contract or Grant No.
Argonne National Laboratory 9700 South Cass Avenue Argonne, Illinois 60439	Interagency Order No. C-91113-D
	13. Type of Report and Period Covered
12. Sponsoring Agency Name and Address	
NASA Lewis Research Center Cleveland, Ohio	14. Sponsoring Agency Code

A X 33 7235

15. Supplementary Notes

16. Abstract

See Attached

17. Key Words (Suggested by Author(s))	18. Distribution Statement
	General Release

19. Security Classif. (of this report)	20. Security Classif. (of this page)	21. No. of pages	22. Price*
Unclassified	Unclassified	26	

*For sale by the National Technical Information Service, Springfield, Virginia 22161